Theranostics

DOI: 10.1002/anie.200703554

Multifunctional Magneto-Polymeric Nanohybrids for Targeted Detection and Synergistic Therapeutic Effects on Breast Cancer**

Jaemoon Yang, Choong-Hwan Lee, Hyun-Ju Ko, Jin-Suck Suh, Ho-Geun Yoon, Kwangyeol Lee, Yong-Min Huh, and Seungjoo Haam**

High-resolution molecular and cellular imaging is one of the most promising applications of nanoparticles, and a number of nanostructured materials, especially of cadmium-containing II–VI semiconductors, have been developed to suit this purpose.[1] Recently, it was demonstrated that magnetic nanoparticles can be utilized as excellent magnetic resonance imaging (MRI) probes for noninvasive in vivo monitoring of molecular and cellular events.[2] We recognized the presence of a number of biocompatible polymers suitable for targeted drug delivery[3] and came upon an idea to combine the magnetic nanocrystals as ultrasensitive MR contrast agents, anticancer drugs as chemotherapeutic agents, and biodegradable amphiphilic block copolymers as stabilizers into a multifunctional hybrid nanosystem. The prepared multifunctional magneto-polymeric nanohybrids (MMPNs) further modified by antibodies would seek cancerous parts and allow simultaneous MR imaging and treatment (Scheme 1). Herein, we report a novel protocol for the preparation of MMPNs and characterization to evaluate the sensitivity and stability of prepared nanohybrids. Furthermore, targeted detection ability by MRI and synergistic tumoricidal efficacy on breast cancer cells were investigated for cellular and animal models.

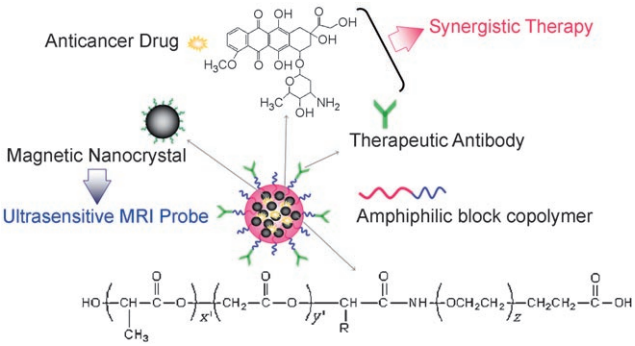

Scheme 1. Schematic illustration for the fabrication of MMPNs.

Monodispersed magnetic nanocrystals, soluble in organic solvents, were synthesized as reported (Figure 1 a,b).[4] To obtain the required water solubility, the hydrophobic nanocrystals and anticancer drug (doxorubicin, DOX) were simultaneously encapsulated with the amphiphilic block copolymer by a nanoemulsion method to give MMPNs.[3e] The structures of MMPNs examined by TEM are shown in Figure 1 c,d, and the sizes of the MMPNs are consistent with the results from laser scattering: 69.7 ± 8.7 nm ($MnFe_2O_4$) and 72.8 ± 9.3 nm (Fe_3O_4), respectively (see the Supporting

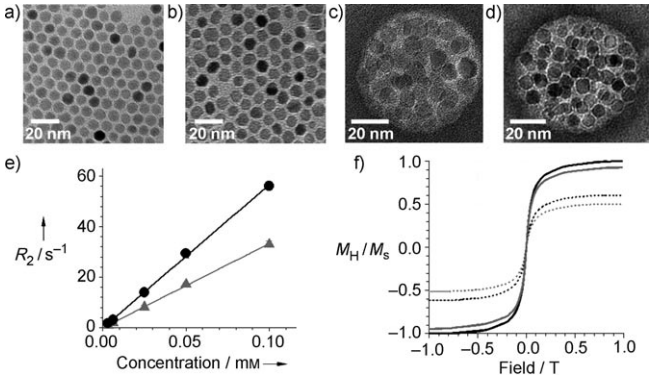

Figure 1. TEM images of magnetic nanocrystals of a) $MnFe_2O_4$ and b) Fe_3O_4 and MMPNs containing c) $MnFe_2O_4$ or d) Fe_3O_4 nanocrystals. e) Graph of relaxivity versus the concentration of MMPNs; $MnFe_2O_4$ (●), Fe_3O_4 (▲). f) Magnetic hysteresis loops of magnetic nanocrystals (solid line) and MMPNs (dashed line); $MnFe_2O_4$ (black) and Fe_3O_4 (gray). M_S is a standard magnetization (80.77 emu g^{-1}); M_H is the magnetization of each of the magnetic nanocrystals and MMPNs

[*] H.-J. Ko, Prof. J.-S. Suh, Prof. H.-G. Yoon, Prof. Y.-M. Huh
Department of Radiology &
Department of Biochemistry and Molecular Biology
Yonsei University
Seoul 120-752 (Korea)
Fax: (+82) 2-312-6401
E-mail: ymhuh@yuhs.ac
Homepage: http://microrxn.yonsei.ac.kr
J. Yang, Prof. S. Haam
Department of Chemical Engineering
Yonsei University
Seoul 120-749 (Korea)
Fax: (+82) 2-312-6401
E-mail: haam@yonsei.ac.kr
C.-H. Lee
Advanced Technology Research Center, ATGen
68 Yatap-dong, Bundang-gu
Seongnam, Gyeonggi, 463-816 (Korea)
Prof. K. Lee
Department of Chemistry
Korea University
Seoul 136-701 (Korea)

[**] We thank Prof. Kunhong Kim at Yonsei University for the insightful discussion. This work was supported by KOSEF through National Core Research Center for Nanomedical Technology (R15-2004-024-00000-0 and R01-2006-000-10023-0, and KOSEF 2007-8-1158), the National R&D Program for Cancer Control, Ministry of Health & Welfare, Republic of Korea (0620190-1).

Supporting information for this article is available on the WWW under http://www.angewandte.org or from the author.

Information). The amount of magnetic nanoparticles in the MMPNs was determined with a thermogravimetric analyzer to be 41.7 wt% ($MnFe_2O_4$) and 40.9 wt% (Fe_3O_4) (see the Supporting Information).

For evaluation of the effectiveness of the diagnostic abilities, we investigated the magnetic properties and induced MR signals of the two types of MMPNs. The spin–spin relaxation time weighted (T_2-weighted) spin–echo MRI of drug-loaded MMPNs showed a significant shift in the lower signal intensity that increased with the concentration of MMPNs (Supporting Information). The relaxivity coefficient of MMPNs containing $MnFe_2O_4$ nanocrystals (567 $mM^{-1}s^{-1}$) was remarkably larger than that of MMPNs with Fe_3O_4 nanocrystals (333 $mM^{-1}s^{-1}$; Figure 1e). Better sensitivity of $MnFe_2O_4$ than Fe_3O_4 in MRI applications has recently been demonstrated for individual nanoparticles.[2d] It was also reported that the MR sensitivity is greatly enhanced by clustering individual magnetic nanocrystals.[5] The hysteresis loops of MMPNs were observed using a vibration sample magnetometer at 300 K (Figure 1f). Our results showed that the MMPNs exhibited superparamagnetic behavior without magnetic hysteresis. The saturation of magnetization values for MMPNs were 48.78 emu g^{-1} ($MnFe_2O_4$) and 40.65 emu g^{-1} (Fe_3O_4) at 1.5 T, which are smaller than those of corresponding magnetic nanoparticles, 80.77 emu g^{-1} ($MnFe_2O_4$) and 73.98 emu g^{-1} (Fe_3O_4), owing to the presence of organic components.

As MR probes in aqueous phase, the MMPNs demonstrated excellent colloidal stability at a high concentration (up to 1 mM of MMPNs), in a wide range of salt concentrations (NaCl, ca. 5 M), and within various pH ranges (from about pH 4 to about pH 12; Supporting Information).

The targeting efficacy of the MMPNs and their detection by MRI were investigated in breast cancer cell lines. The human epidermal growth factor receptor 2 (HER2) was used as a tumor-targeting marker for the treatment of patients with metastatic breast cancer.[6] Fibroblast NIH3T6.7 cells, which highly express the HER2/neu cancer markers, were compared with MDA-MB-231 cells, which express low levels of the cancer markers.[2d] To compare the performance of MMPNs in these cell lines, MMPNs with $MnFe_2O_4$ nanoparticles were conjugated with anti-HER antibody (HER, herceptin) by utilizing the carboxyl group on the surface of the MMPNs. The difference of $\Delta R_2/R_2^{\text{nontreated}}$ ($R_2 = T_2^{-1}$) in cells treated with HER-conjugated MMPNs (HER-MMPNs) compared to those of MMPNs conjugated with an irrelevant antibody (IRR, human IgG; IRR-MMPNs) were about 320% (NIH3T6.7) and about 57% (MDA-MB-231), respectively (Figure 2a). In addition, HER-MMPNs exhibited specific affinity (4.4 times) for NIH3T6.7 cells compared with MDA-MB-231 cells, demonstrating the efficient targeted delivery of MMPNs for the HER2/neu receptor. IRR-MMPN-treated cells, however, showed partial enhancement against the MR signal intensity owing to nonspecific binding.[7]

The fluorescence intensity of NIH3T6.7 cells treated with HER-MMPNs was larger than that of MDA-MB-231 cells (Supporting Information). In addition, the confocal microscopic images showed that NIH3T6.7 cells incubated with HER-MMPNs presented excellent uptake efficiency compared to other cases (Figure 2b–e). In the case of NIH3T6.7 cells treated with HER-MMPNs, a bright green color was observed in the microscopic image, whereas faint green fluorescence was noted for the IRR-MMPNs. These flow cytometry analysis and microscopic results demonstrated that HER-MMPNs successfully bind to NIH3T6.7 cells and are subsequently taken into the cells.

To assess the therapeutic potential for the combination of therapeutic antibodies and chemotherapeutic drugs, the degree of drug release and the inhibition of cell growth were investigated. The amount of DOX in the HER-MMPNs and entrapment efficiency were 3.3 wt% and 71.4%, respectively. These results were similar to those of the MMPNs: 3.5 wt% (amount of DOX in the MMPNs) and 73.5% (entrapment efficiency). Drug-release data from the prepared MMPNs and HER-MMPNs are shown in Figure 2f. The release test was performed in triplicate, and the obtained values were used to calculate a mean value and standard deviation. After 3 and 12 days, 60% and 80% of the encapsulated DOX was released from the MMPNs and HER-MMPNs, respectively, owing to polymer degradation.

We next determined the in vitro differential cytotoxicity of HER-MMPNs, IRR-MMPNs, and HER-MNPs (HER

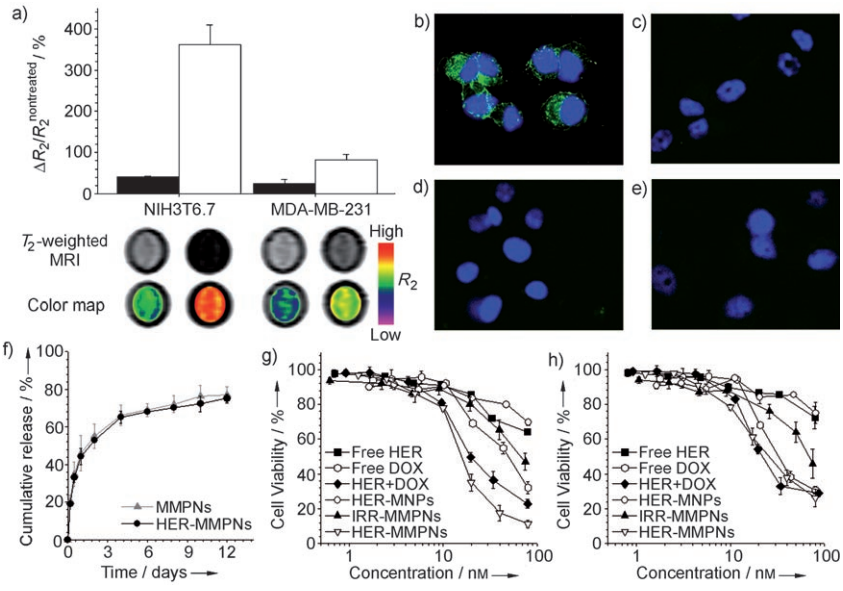

Figure 2. a) The T_2-weighted MR images, their color maps and graph of $\Delta R_2/R_2^{\text{nontreated}}$ value for NIH3T6.7 and MDA-MB-231 cells (IRR-MMPNs; black, HER-MMPNs; white). b,c) Confocal microscopic images of NIH3T6.7 cells incubated with HER-MMPNs (b), IRR-MMPNs (c); d,e) MDA-MB-231 cells incubated with HER-MMPNs (d) and IRR-MMPNs (e). f) Drug-release profile of MMPNs and HER-MMPNs for 12 days. g,h) Cell-viability test of NIH3T6.7 (g) and MDA-MB-231 cells (h) by MTT assay; treated with free DOX, free HER, DOX + HER, HER-MNPs, IRR-MMPNs, and HER-MMPNs (equivalent amount of HER and DOX).

conjugated with a non-drug-loaded magnetic nanoparticle–polymer hybrid) using an MTT assay on NIH3T6.7 and MDA-MB231 cells, compared to those of DOX + HER, free HER, and free DOX. Cells were incubated for 4 h with those prepared samples.[8] After the initial incubation period, the cells were washed and incubated further for 72 h. The cell viabilities are presented as the ratio of the number of live cells incubated under the above conditions to the number of nontreated control cells (Figure 2g,h). Our data show that HER-MMPNs are remarkably more cytotoxic than the conventional combination of DOX + HER (11.3 ± 3.2 % vs. 22.9 ± 1.4 %, respectively) on NIH3T6.7 cells whereas HER-MMPNs did not have a different effect on MDA-MB231 cells (25.8 ± 5.2 % vs. 28.6 ± 2.0 %, respectively) at equivalent DOX concentration (80 nM). These noticeable results show that HER-MMPNs easily enter into the intracellular cytoplasm by a tumor-target-mediated endocytosis pathway and efficiently release DOX. The cytotoxicity is further enhanced by the additional inhibitory effect of HER on cell growth and proliferation. Furthermore, we observed that the cytotoxic effect of HER-MMPNs was larger than the combined effect of both HER-MNPNs and IRR-MMPNs (11.3 ± 3.2 % vs. 16.7 ± 3.3 %, respectively). This enhanced efficacy indicates that effects of HER and DOX mediated by MMPNs are synergistic, thus making HER-MMPNs effective for the treatment of breast cancer.

We further investigated the MR images of an in vivo mouse model using well-dispersed aqueous MMPNs as smart contrast agents for breast cancer detection. In a set of nude mice, subjects were implanted in their proximal thigh region with NIH3T6.7 cell lines. MR imaging of the mice was performed at different temporal points (preinjection, postinjection (immediately, 4 h, and 12 h) after the intravenous tail injection of the HER-MMPNs (120 μg Fe + Mn; Figure 3a–h). After injection of the HER-MMPNs, an immediate color change to black was evident, and a continuous $\Delta R_2/R_2^{pre}$ value increase of about 50.5 % was observed after injection and about 23.2 % at 12 h. The T_2-weighted MR images for IRR-MMPNs, which were used as a control ($\Delta R_2/R_2^{pre}$ value increase of about 14.4 % after injection and about 6.2 % at 12 h), were consistent with previous in vitro studies and showed a mild enhanced permeability and retention (EPR) effect on the tumor site. These results imply that the HER-MMPNs as MR probes make it possible to actively reach and effectively bind to the target cancer cells of the proximal thigh region.

For investigation of therapeutic efficacy of our HER-MMPNs, the tumor growth rate of an animal model xenografted with NIH3T6.7 cells was evaluated. After tumors had developed to a size of about 90 mm^3, we performed comparative efficacy studies by dividing animals into seven groups ($n = 3$, where n is the number of mice in each group). As shown in Figure 3j, both HER-MMPNs and IRR-MMPNs groups demonstrated remarkable tumor growth inhibition efficacy as compared with each control group (nontreated, DOX, HER, DOX + HER, and HER-MPNs). The growth of tumor cells was more rapid than for normal cells, and more neoangiogenic vessels of tumor tissue were generated to supply the oxygen and nutritive elements. Thus, the tumor should have fallen into necrosis or apoptosis because of minimal vascular supplying parts.[9] Consequently, nanometer-sized MMPNs could be taken up by tumor cells in comparison with normal tissue, and IRR-MMPNs (77.3 ± 6.2 nm) could exhibit inhibition effects owing to an EPR effect. Interestingly, HER-MMPNs (79.3 ± 7.9 nm) demonstrated more effective tumor growth inhibition than IRR-MMPNs. These noticeable results suggested that injected HER-MMPNs were target-specifically delivered to overexpressed HER2/neu receptors of NIH3T6.7 cells in the mouse model and were taken up by a receptor-mediated endocytosis process. Release of DOX from the HER-MMPNs demonstrated exceptional therapeutic efficacy.

In summary, we have developed multifunctional magneto-polymeric nanohybrids (MMPNs) composed of magnetic nanocrystals and anticancer drugs encapsulated by an amphiphilic block copolymer. The antibody-modified MMPNs (HER-MMPNs) demonstrated ultrasensitive targeted detection by MRI in in vitro and in vivo models. In addition, the HER-MMPNs showed excellent synergistic effects for the inhibition of tumor growth. This study may be used as a foundation for the development of novel nanodrugs for the simultaneous diagnosis and treatment of various types of cancers.

Received: August 6, 2007
Published online: October 17, 2007

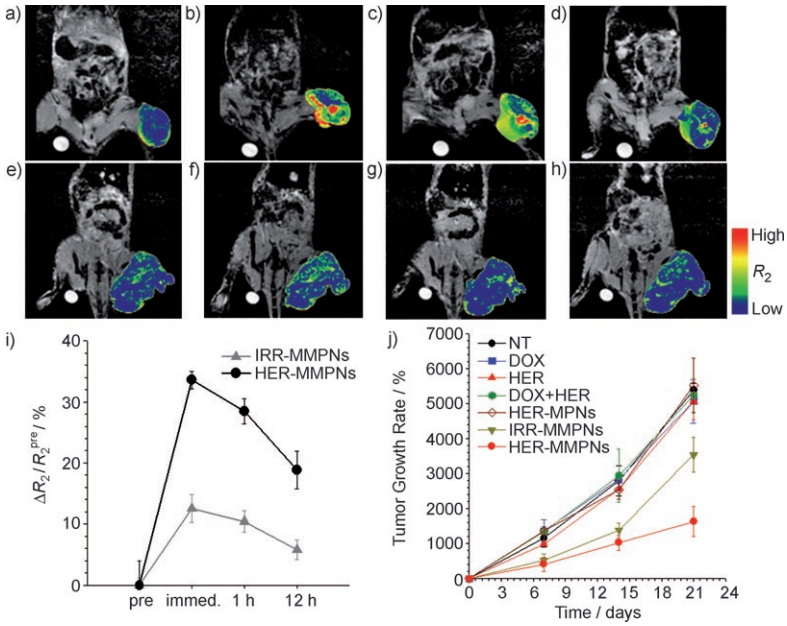

Figure 3. MR images and their color maps (tumor region) of cancer-targeting events of HER-MMPNs (a–d) and IRR-MMPNs (e–h) in NIH3T6.7 cells implanted in mice at various time intervals: a,e) preinjection; b,f) immediately; c,g) 1 h; d,h) 12 h after injection of the MMPNs. i) $\Delta R_2/R_2^{pre}$ graph versus time before and after injection of MMPNs. j) Comparative therapeutic-efficacy study in an in vivo model.

Keywords: drug delivery · hybrid composites · imaging agents · magnetic resonance · transmission electron microscopy

[1] a) A. P. Alivisatos, *Science* **1996**, *271*, 933 – 937; b) R. E. Bailey, S. Nie, *J. Am. Chem. Soc.* **2003**, *125*, 7100 – 7106; c) S. Kim, B. Fisher, H.-J. Eisler, M. Bawendi, *J. Am. Chem. Soc.* **2003**, *125*, 11466 – 11467; d) S. Kim, Y. T. Lim, E. G. Soltesz, A. M. De Grand, J. Lee, A. Nakayama, J. A. Parker, T. Mihaljevic, R. G. Laurence, D. M. Dor, L. H. Cohn, M. G. Bawendi, J. V. Frangioni, *Nat. Biotechnol.* **2004**, *22*, 93 – 97; e) B.-S. Kim, J. M. Qiu, J. P. Wang, T. A. Taton, *Nano Lett.* **2005**, *5*, 1987 – 1991.

[2] a) Y. Jun, Y.-M Huh, J. Choi, J. Lee, H. Song, S. Kim, S. Yoon, S. Kim, J. Shin, J. Suh, J. Cheon, *J. Am. Chem. Soc.* **2005**, *127*, 5732 – 5733; b) D. Artemov, N. Mori, B. Okollie, Z. M. Bhujwalla, *Magn. Reson. Med.* **2003**, *49*, 403 – 408; c) Y.-M Huh, Y. Jun, H. Song, Kim, S. J. Choi, J. Lee, S. Yoon, K. Kim, J. Shin, J. Suh, J. Cheon, *J. Am. Chem. Soc.* **2005**, *127*, 12387 – 12391; d) J. Lee, Y.-M Huh, Y. Jun, J. Seo, J. Jang, H. Song, S. Kim, E. Cho, H. Yoon, J. Suh, J. Cheon, *Nat. Med.* **2007**, *13*, 95 – 99.

[3] a) X. Michalet, F. F. Pinaud, L. A. Bentolila, J. M. Tsay, S. Doose, J. J. Li, G. Sundaresan, A. M. Wu, S. S. Gambhir, S. Weiss, *Science* **2005**, *307*, 538 – 544; b) O. C. Farokhzad, J. Cheng, B. A. Teply, I. Sherifi, S. Jon, P. W. Richie, J. P. Kantoff, R. Langer, *Proc. Natl. Acad. Sci. USA* **2006**, *103*, 6315 – 6320; c) S. Sengupta, D. Eavarone, I. Capila, G. Zhao, N. Watson, T. Kiziltepe, R. Sasisekharan, *Nature* **2005**, *436*, 568 – 572; d) H. Wartlick, K. Michaelis, S. Balthasar, K. Strebhardt, J. Kreuter, K. Langer, *J. Drug Targeting* **2004**, *12*, 461- 471; e) J. Yang, S. B. Park, H. G. Yoon, Y.-M. Huh, S. Haam, *Int. J. Pharm.* **2006**, *324*, 185 – 190; f) A. Koide, A. Kishimura, K. Osada, W.-D. Jang, Y. Yamasaki, K. Kataoka, *J. Am. Chem. Soc.* **2006**, *128*, 5988 – 5989.

[4] S. Sun, H. Zeng, D. B. Robinson, S. Raoux, P. M. Rice, S. X. Wang, G. Li, *J. Am. Chem. Soc.* **2004**, *126*, 273 – 279.

[5] a) J. M. Perez, L. Josephson, T. O'Loughlin, D. Hogemann, R. Weissleder, *Nat. Biotechnol.* **2002**, *20*, 816 – 820; b) J.-F. Berret, N. Schonbeck, F. Gazeau, D. El Kharrat, O. Sandre, A. Vacher, M. Airiau, *J. Am. Chem. Soc.* **2006**, *128*, 1755 – 1761.

[6] R. M. Hudziak, G. D. Lewis, M. Winget, B. M. Fendly, H. M. Shepard, A. Ullrich, *Mol. Cell. Biol.* **1989**, *9*, 1165 – 1172.

[7] A. K. Iyer, G. Khaled, J. Fang, H. Maeda, *Drug Discovery Today* **2006**, *11*, 812 – 818.

[8] a) P. R. Mishra, N. K. Jain, *Drug Delivery* **2003**, *10*, 277 – 282; b) M. Kovar, T. Mrkvan, J. Strohalm, T. Etrych, K. Ulbrich, M. Stastny, B. Rihova, *J. Controlled Release* **2003**, *92*, 315 – 330; c) H. S. Yoo, J. E. Oh, K. H. Lee, T. G. Park, *Pharm. Res.* **1999**, *16*, 1114 – 1118; d) S. Q. Liu, Y. W. Tong, Yi-Yan Yang, *Biomaterials* **2005**, *26*, 5064 – 5074; e) H. S. Yoo, T.G Park, *J. Controlled Release* **2001**, *70*, 63 – 70.

[9] a) Z. Li, L. Wei, M. Gao, H. Lei, *Adv. Mater.* **2005**, *17*, 1001 – 1007; b) C. A. Cuenod, L. Fournier, D. Balvay, J.-M. Guinebretière, *Abdom. Imaging* **2006**, *31*, 188 – 194.

